Journal of
Materials in Life Sciences

Vol. 4 No. 1 (2025)

Full Paper

Synthesis and Characterization of Novel Mesostructured TUD-C Supported Copper-doped Titanium Dioxide Photocatalyst

Chee Chuan Tan[a], Ching Shien Lee[a], Siew Ling Lee[a,b,*]

[a]Department of Chemistry, Faculty of Science, Universiti Teknologi Malaysia, 81310 UTM Johor Bahru, Johor, Malaysia.
[b]Centre for Sustainable Nanomaterials, Universiti Teknologi Malaysia, 81310 UTM Johor Bahru, Johor, Malaysia.

Article history
Received
18 April 2025
Revised
09 May 2025
Accepted
26 May 2025
Published online
31 May 2025

*Corresponding author
lsling@utm.my

Abstract

Titanium dioxide (TiO_2) photocatalyst has garnered extensive applications owing to its excellent chemical stability and cost-effectiveness. Nonetheless, its practical efficiency is hindered by several intrinsic limitations, including a relatively wide band gap, rapid recombination of photoinduced electron-hole pairs, and a limited surface area, all of which significantly diminish its photocatalytic efficiency. To address these shortcomings, a series of novel copper-doped titania photocatalysts supported on Technische Universiteit Delft-Crystalline (TUD-C), denoted as xCu-TiO_2@TUD-C (x = 0.1–1.0 mol%), were synthesized. These photocatalysts were fabricated through a multistep process involving sol-gel synthesis, hydrothermal treatment, wet impregnation, and calcination. Powder X-ray diffraction (PXRD) analysis confirmed that the TiO_2 component crystallized in the anatase phase. Additionally, PXRD verified that the TUD-C support retained the Modernite Framework Inverted (MFI) zeolitic structure, along with a high specific surface area ranging between 270 and 321 m²/g. The successful incorporation of Cu-doped TiO_2 onto the TUD-C support was validated through energy-dispersive X-ray (EDX) elemental analysis. Furthermore, diffuse reflectance ultraviolet-visible (DRUV-Vis) spectroscopy revealed a noticeable reduction in band gap energies for the 0.1, 0.5, and 0.7 mol% Cu-TiO_2@TUD-C samples, which exhibited values of 2.93 eV, 3.06 eV, and 2.77 eV, respectively, lower than that of undoped TiO_2 (3.29 eV). These findings underscore the promising potential of the synthesized Cu-TiO_2@TUD-C materials as efficient visible-light-responsive photocatalysts for photodegrading various organic pollutants.

Keywords titanium dioxide, copper, TUD-C, mesoporous, photocatalyst

1.0 INTRODUCTION

Titanium dioxide (TiO_2) exists in three predominant polymorphic forms: anatase, brookite, and rutile [1]. Its cost-efficiency, non-toxic nature, and outstanding photocatalytic capabilities have driven extensive research into its potential applications, particularly in wastewater remediation and various industrial processes [2–4]. However, the photocatalytic efficiency of TiO_2 is hindered by inherent limitations such as a wide band gap, its restriction to UV-light activation, a high rate of photogenerated electron-hole recombination, and a relatively low surface area [5]. To overcome these drawbacks, metal doping, particularly with copper (Cu), has emerged as a promising strategy to enhance the photocatalytic efficiency of TiO_2, as supported by numerous studies [3].

Cu has received considerable attention for its potential use in photocatalytic systems, both in its elemental form and as a metal oxide. Its appeal lies in its affordability, high redox potential, superior electrical conductivity, and ability to promote diverse redox reactions due to its variable oxidation states [6,7]. Besides, it serves as an effective dopant for TiO_2 due to its atomic radius being comparable to that of titanium, allowing it to integrate seamlessly into the TiO_2 lattice [8]. Within the TiO_2 matrix, Cu facilitates the capture and transfer of photoexcited electrons across the material's surface, thereby enhancing charge separation. Owing to these properties, Cu is frequently employed as a dopant in the synthesis of TiO_2, as it significantly augments the material's photocatalytic activity [8,9]. Copper acts as an effective electron acceptor, reducing electron-hole recombination, and shifts the optical absorption of TiO_2 into the visible light spectrum, enabling the catalyst to function under visible light irradiation [9,10].

Technische Universiteit Delft-Crystalline (TUD-C) represents an emerging mesoporous support material, characterized by integrating mesoporous silica with a Modernite Framework Inverted (MFI) zeolitic structure. Furthermore, the incorporation of a one-step modification approach, derived from the synthesis of Technische Universiteit Delft-1 (TUD-1), simplifies TUD-C production through the addition of an alumina source, eliminating the need for surfactants [11,12]. TUD-C boasts several advantageous features, including a three-dimensional sponge-like pore architecture, strong acidity, high surface area, excellent thermal and structural stability, and uniform pore size distribution [11,12]. The enhanced surface area of TUD-C effectively compensates for the limited surface-active sites of TiO_2. Nevertheless, investigations into TUD-C as a catalyst support remain relatively scarce, warranting further exploration to fully realize its functional and practical potential [5,11,12].

This study presents the development of a novel Cu-TiO_2@TUD-C composite material. The structural and physicochemical characteristics of the synthesized photocatalysts are systematically examined and discussed.

2.0 EXPERIMENTAL

2.1 Materials

Titanium isopropoxide (TTIP), acetylacetone (acac), and tetraethylammonium hydroxide (TEAOH) were purchased from Sigma-Aldrich, while absolute ethanol (EtOH) was supplied by Hayman Limited. Tetraethyl orthosilicate (TEOS) and triethanolamine (TEA) were purchased from Qrec and Merck, respectively. Copper nitrate trihydrate ($Cu(NO_3)_2{\cdot}3H_2O$) was used as copper dopants, whereas Zeolite Socony Mobil-5 (ZSM-5) from Acros Organics was used as the zeolitic precursor.

2.2 Preparation of Materials

A series of Cu-TiO_2@TUD-C photocatalysts with varying copper dopant concentrations (in mol%) was synthesized. The preparation involved a combination of chemical techniques, including calcination, hydrothermal treatment, sol-gel synthesis, and wet impregnation. For comparative analysis, pure TiO_2 and TUD-C were also synthesized under similar conditions. All chemicals employed in the synthesis processes were used as received, without further purification.

TiO_2 was synthesized using titanium isopropoxide (TTIP) as the precursor via the sol-gel method. Absolute ethanol serving acetylacetone (acac) were used as the solvent and the chelating agent, respectively. The components were mixed in a molar ratio of 1 TTIP: 100 EtOH: 2 acac, yielding a clear, light-yellow solution (denoted as Solution A). Solution A was stirred at room temperature for 2 h, followed by evaporation at 80°C and drying at 110 °C overnight. The resulting solid was calcined at 500 °C for 5 h to obtain TiO_2. For the preparation of copper-doped titania, an aqueous solution of copper nitrate (2 mL) was added dropwise into Solution A. The resulting mixture was stirred for 2 h, followed by the same evaporation, aging, and calcination procedures. Copper dopant concentrations were varied at 0.1, 0.3, 0.5, 0.7, and 1.0 mol%.

In this study, TUD-C functioned as the mesoporous zeolitic support for the photocatalyst. Its synthesis was carried out via a sol-gel process followed by hydrothermal treatment, utilizing TEAOH and TEA as structure-directing agents. The precursor solution was prepared using distilled water, tetraethyl orthosilicate (TEOS), TEA, TEAOH, and ZSM-5 in a molar ratio of 11 H_2O: 1 TEOS: 0.5 TEA: 0.1 TEAOH: 0.1 ZSM-5. A Si/Al molar ratio of 30 was maintained, and the resulting material was designated TUD-C (30). Initially, distilled water and TEA were mixed and stirred for 1 h to form Solution B, while TEOS and ZSM-5 were simultaneously mixed and stirred for 1 h to form Solution C. Solution B was then added dropwise to Solution C, yielding Solution D, which was stirred for another 1 h to ensure complete homogenization. TEAOH was subsequently added dropwise to Solution D, followed by 2 h of stirring. The final mixture was aged at room temperature for 24 h to produce a solid gel, which was then ground into fine powder. After a hydrothermal treatment at 130°C for 10 h, the powder was dried at 130°C and calcined in air at 800°C for 6 h to remove any organic residues.

To synthesize the Cu-TiO_2@TUD-C composite photocatalysts, the pre-formed Cu-TiO_2 powder was incorporated into the TUD-C precursor mixture. The suspension was stirred for 2 h before undergoing the same aging and evaporation processes as previously described. The final products were labelled as *x*Cu-TiO_2@TUD-C, where *x* indicates the specific copper dopant loading.

2.3 Characterization of Materials

All samples were subjected to comprehensive characterization techniques, including Powder X-Ray Diffraction (XRD), Diffuse Reflectance UV-Visible (DRUV-Vis) Spectroscopy, Fourier Transform Infrared (FTIR) Spectroscopy, nitrogen adsorption-desorption surface area analysis, and Field Emission Scanning Electron Microscopy (FESEM) coupled with Energy Dispersive X-ray (EDX) analysis. XRD patterns were obtained using a Bruker D8 Advance diffractometer equipped with Cu Kα radiation (λ = 1.5418 Å), operated at 40 mA and 40 kV. The finely ground powder (about 1 g) was analyzed under ambient conditions over a 2θ range of 20° to 90°, applying a step time of 1 s and a step size of 0.02°. DRUV-Vis spectroscopy was performed using a PerkinElmer Lambda 900 UV-Vis spectrophotometer, fitted with a diffuse reflectance accessory and a 76 mm integrating sphere. Barium sulphate served as the reference standard. Measurements were carried out over a wavelength range of 190–800 nm, with a frequency of 200 Hz and a power output of 550 W.

For FTIR analysis, approximately 20 mg of each synthesized sample was thoroughly mixed with 2000 mg of anhydrous potassium bromide (KBr) in a 1:100 mass ratio, then ground into a fine powder. The mixture was pressed into 13 mm pellets under a pressure of 10 tons for 5 minutes, yielding self-supporting discs. Spectral data were acquired using a Thermo Scientific Nicolet iS10 spectrometer ranging 400–4000 cm^{-1}. Nitrogen adsorption-desorption measurements were conducted at −196 °C using a Thermo Fisher Scientific Sorptomatic 1990 surface area analyzer to determine surface area, pore volume, and porosity. Before analysis, the samples were degassed at 250 °C for 16 hours. The BET method was applied for specific surface area determination, while pore size distribution was analyzed using the Barrett-Joyner-Halenda (BJH) method. The surface morphology of the Cu-TiO_2@TUD-C photocatalyst was examined using a JEOL JSM-6701F field emission scanning electron microscope, capable of resolutions up to 1 nm at 15 kV and 2.2 nm at 1 kV, with a maximum probe current of 2 nA.

3.0 RESULTS AND DISCUSSION

3.1 Synthesis of the TUD-C Supported Cu-TiO_2 Photocatalysts

A series of samples were successfully prepared, including TUD-C (Si/Al = 30), 0.1Cu-TiO_2@TUD-C, 0.3Cu-TiO_2@TUD-C, 0.5Cu-TiO_2@TUD-C, 0.7Cu-TiO_2@TUD-C, and 1.0Cu-TiO_2@TUD-C. After the calcination process, which removed the organic substances, white powder TUD-C and creamy white Cu-TiO_2@TUD-C powders were obtained.

3.2 Synthesis of the TUD-C Supported Cu-TiO_2 Photocatalysts

3.2.1 Powder XRD

Powder X-ray diffraction (XRD) analysis was employed to determine the crystallinity and phase purity of all the synthesized samples. Figure 1(a) presents the XRD patterns of pure TiO_2, 1.0Cu-TiO_2, pure TUD-C, and 1.0Cu-TiO_2@TUD-C. The TiO_2 synthesized via the sol-gel method exhibited diffraction peaks corresponding to the anatase phase with a tetragonal crystal structure, as referenced in JCPDS No. 84-1286 [13]. A prominent peak at 2θ = 25.21° was observed and indexed as the (101) reflection, along with several less intense peaks at 36.92°, 37.73°, 38.39°, 47.96°, 54.13°, 55.06°, 62.56°, 68.83°, and 75.02°, corresponding to the (103), (004), (112), (200), (105), (211), (204), (116), and (215) planes, respectively. These patterns confirm the formation of anatase TiO_2. The XRD pattern of the 1.0Cu-TiO_2 sample closely resembled that of pure anatase TiO_2, suggesting that the anatase structure remained intact following the incorporation of copper. Additionally, the presence of monoclinic CuO was confirmed by several minor peaks at 2θ values of 32.53°, 35.58°, 38.78°, 48.79°, 58.23°, 61.59°, 66.36°, 68.03°, 72.45°, and 75.12°, corresponding to JCPDS No. 48-1548 [14]. For the TUD-C sample, two significant peaks around 2θ = 25° indicated the presence of aluminium silicate species and ZSM-5 zeolitic structure [4].

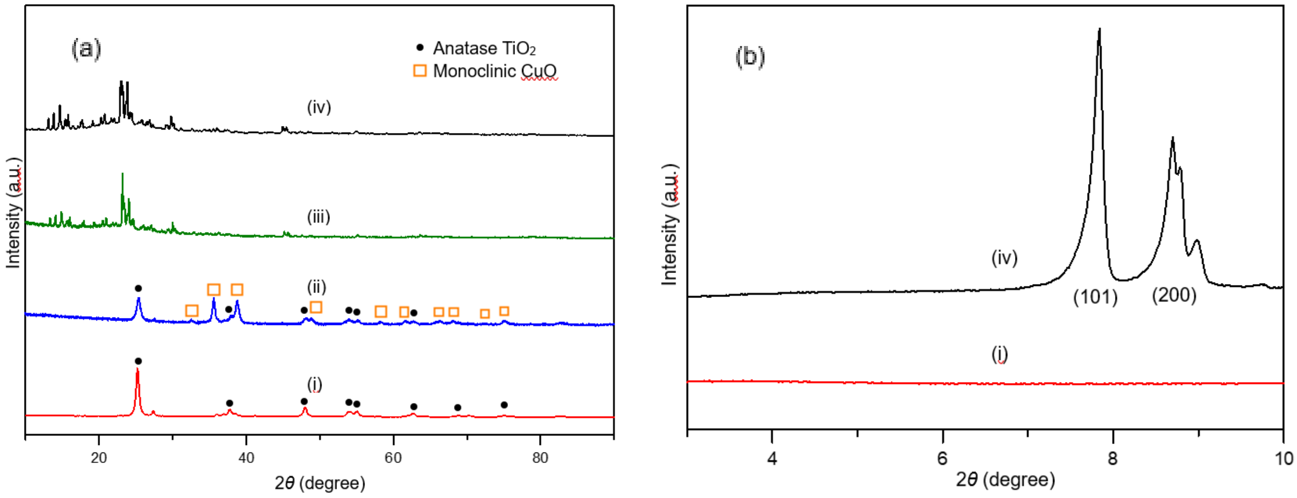

F

Figure 1 (a) Wide-angle XRD patterns and (b) low-angle XRD patterns of (i) pure TiO_2, (ii) 1.0Cu-TiO_2, (iii) pure TUD-C, and (iv) 1.0Cu-TiO_2@TUD-C

As shown in Figure 1(a), the successful incorporation of Cu-TiO_2 into the TUD-C support was evident, as key diffraction peaks characteristic of the MFI zeolitic framework were still discernible in the 1.0Cu-TiO_2@TUD-C sample. Furthermore, peaks that were attributed to the anatase TiO_2 remained detectable, albeit with reduced intensity. This diminished intensity was attributed to the substantial difference in the weight ratio between Cu-TiO_2 and TUD-C (1:30), indicating the dominant presence of TUD-C. In Figure 1(b), two distinctive peaks at 2θ = 7.83° and 8.69°, indexed as the (101) and (200) phases, respectively, confirmed the presence of the MFI zeolite framework embedded within the amorphous silica matrix of the Cu-TiO_2@TUD-C [4,11,12]. Crystallite sizes were estimated using the Scherrer equation, with the calculated values summarized in Table 1. The crystallite size of 1.0Cu-TiO_2 was found to be 10.74 nm, which was smaller than that of the pure TiO_2 (18.14 nm). This suggested that CuO integration into the TiO_2 lattice reduced particle growth [15]. Meanwhile, the crystallite size of 1.0Cu-TiO_2@TUD-C (63.51 nm) was comparable to that of pure TUD-C (63.16 nm), indicating that Cu-TiO_2 was effectively incorporated into or onto the TUD-C framework without significantly altering its structural dimensions.

Table 1 Crystallite size of pure TiO_2, 1.0Cu-TiO_2, pure TUD-C, and 1.0Cu-TiO_2@TUD-C

Sample	Crystallite size (nm)
TiO_2	18.14
1.0Cu-TiO_2	10.74
TUD-C	63.16
1.0Cu-TiO_2@TUD-C	63.51

3.2.2 DR UV-Vis Spectroscopy

Diffuse Reflectance UV-Visible (DRUV-Vis) spectroscopy was used to explore the optical properties of the synthesized pure TiO_2 and a series of Cu-TiO_2@TUD-C composites with varying copper dopant concentrations. The DRUV-Vis spectra of all synthesized materials are depicted in Figure 2.

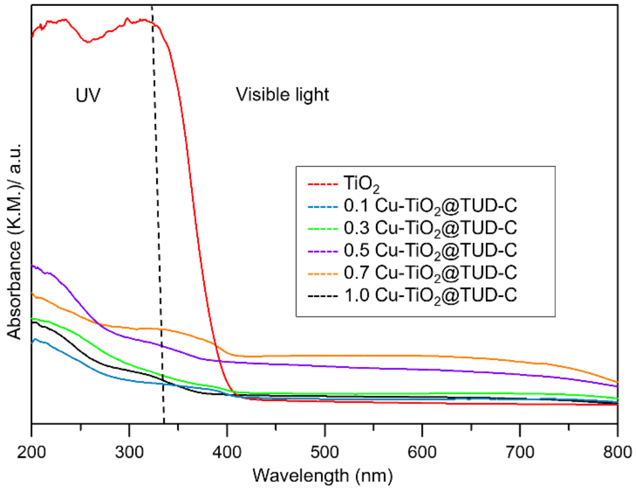

Figure 2 DR UV-Vis absorption spectra of synthesized materials with different molar percentages of Cu dopant

For the pure TiO_2 sample, two prominent absorption bands were observed at 235 nm and 330 nm. The former is attributed to hydrated tetrahedrally coordinated titanium species (Ti^{4+}), while the latter corresponds to octahedrally coordinated or polymeric titanium species, denoted as $(Ti–O–Ti)_n$ [11]. All Cu-TiO_2@TUD-C samples exhibited a noticeable blue shift at the 235 nm absorption band relative to pure TiO_2, signifying successful copper incorporation. Additionally, a subtle absorption shoulder around 330 nm was present in all samples, further indicating the persistence of titanium species in the composite structure. It was also observed that the overall UV absorbance of the Cu-TiO_2@TUD-C composites was significantly reduced compared to that of pure TiO_2, which may be attributed to the dispersion or surface interaction of Cu-TiO_2 within the TUD-C support matrix. Interestingly, UV absorbance increased progressively with copper loading from 0.1 to 0.5 mol%, suggesting enhanced light-harvesting capability. However, a subsequent decline in absorption intensity was recorded for samples containing 0.7 and 1.0 mol% Cu, possibly due to dopant saturation or agglomeration effects that hinder optical performance.

The band gap energy (E_g) of the synthesized materials was determined using the Tauc equation in conjunction with the Kubelka-Munk function. A plot of $[FR_xhv]^2$ versus photon energy (hv) was constructed, and the direct band gap values were obtained by extrapolating the linear portion of the curve to the energy axis. Figure 3 illustrates the corresponding $[FR_xhv]^2$ versus energy (eV) graph, while Table 2 summarizes the calculated E_g, values for the samples. Among the Cu-TiO_2@TUD-C composites, only the 0.1, 0.5, and 0.7 mol% Cu-loaded samples exhibited lower band gap energies than that of pristine TiO_2, which was measured at 3.2 eV. Conversely, the 0.3 and 1.0Cu-TiO_2@TUD-C samples showed slightly higher band gap values. It is noteworthy that the variation in E_g values did not follow a consistent trend with increasing Cu dopant concentration. This irregularity may be attributed to inconsistencies in reaction times during synthesis or to the presence of residual impurities, potentially stemming from incomplete evaporation of acetylacetone during the preparation of Cu-TiO_2. Nevertheless, the reduced E_g values may be attributed to the incorporation of Cu^{2+} ions into the host lattice, and this substitution also introduces a new electronic energy level near the conduction band edge of TiO_2, which facilitates the formation of O_2^- species, because of the charge compensation effects [16].

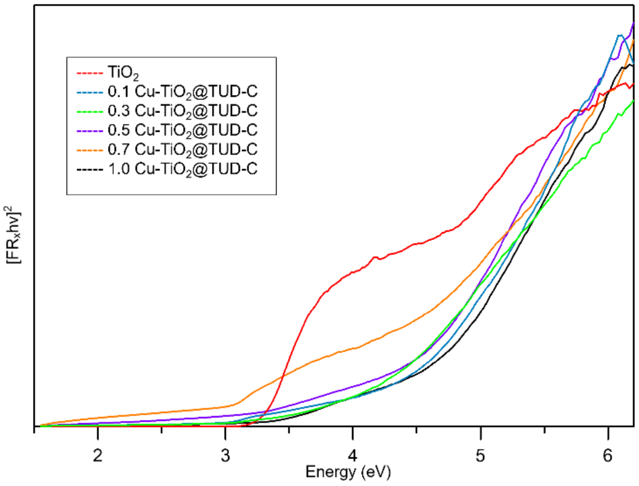

Figure 3 Graph of $[FR_x hv]^2$ against eV of the synthesized samples using the Tauc equation and Kubelka-Munk function

Table 2 Band gap energy of the pure TiO_2 and different mol% Cu-TiO_2@TUD-C samples

Sample	**Calculated direct bandgap energy, E_g, (eV)**
TiO_2	3.29
0.1 Cu-TiO_2@TUD-C	2.93
0.3 Cu-TiO_2@TUD-C	3.33
0.5 Cu-TiO_2@TUD-C	3.06
0.7 Cu-TiO_2@TUD-C	2.77
1.0 Cu-TiO_2@TUD-C	3.37

3.2.3 Fourier Transform Infrared (FTIR) Spectroscopy

FTIR analysis was conducted to examine the functional groups present in the materials. Figure 4 displays the FTIR spectra of pure TiO_2, 1.0Cu-TiO_2, pure TUD-C, and 1.0Cu-TiO_2@TUD-C samples.

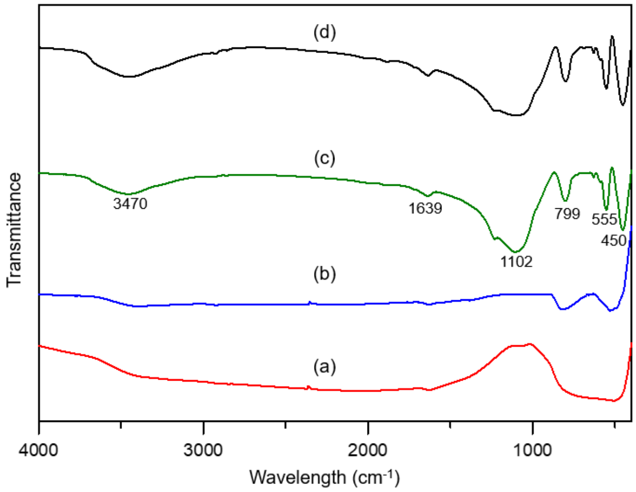

Figure 4 FTIR spectra of (a) pure TiO_2, (b) 1.0Cu-TiO_2, (c) pure TUD-C, and (d) 1.0Cu-TiO_2@TUD-C samples

The spectrum of the 1.0Cu-TiO_2@TUD-C sample exhibited a broad absorption band in the region of 3400–3600 cm^{-1}, along with a minor peak at 1639 cm^{-1}. These features are due to the O–H stretching and bending vibrations, respectively, indicating the presence of surface-adsorbed hydroxyl groups (–OH) from moisture [17,18]. Additionally, the 1.0Cu-TiO_2@TUD-C sample revealed several characteristic absorption bands corresponding to the ZSM-5 zeolitic framework. Notable peaks were detected at 450 cm^{-1}, 555 cm^{-1}, 799 cm^{-1}, and 1102 cm^{-1}, which are associated with T–O bending vibrations (T = Si or Al), MFI framework skeletal vibrations, external symmetric stretching of Si–O–Si, and internal symmetric stretching of Si–O–Si, respectively [5,11]. Furthermore, the band at 1230 cm^{-1}, associated with asymmetric stretching of T–O (T = Si or Al), provided additional evidence of the ZSM-5 structure [5,11]. This vibrational mode is known to be structure-sensitive and is linked to external connectivity between TO_4 tetrahedra.

The intensity of the zeolitic peaks attributed to TUD-C exhibited a noticeable reduction, with minimal or no peak shifts observed following the impregnation of the Cu-TiO_2 sample. This attenuation in intensity can be attributed to the interaction of SiO_2 with the formation of Ti–O–Si and Cu–O–Si linkages. A shift in the band near 965 cm^{-1}, along with the diminished peak intensity, serves as indirect evidence for the presence of Ti–O–Si and Cu–O–Si bonds, which are further associated with the bending vibrations of Si–OH groups. However, the characteristic peak for Ti–O–Si and Cu–O–Si at 965 cm^{-1} did not appear distinctly and instead manifested as a weak shoulder, likely due to overlapping with the broader Si–O–Si band centred at 1102 cm^{-1} [5,11,19]. Additionally, several faint and narrowly defined absorption bands appeared within the 400–800 cm^{-1} region, which are caused by the overlapping skeletal vibrations of bulk TiO_2 and Cu–O stretching modes. Specifically, bands at 580 and 760 cm^{-1} correspond to O–Ti–O and Ti–O–Ti linkages, while peaks located at 483, 517, and 584 cm^{-1} are indicative of Cu–O stretching vibrations [5,11].

3.2.4 Nitrogen Adsorption-Desorption Surface Area Analysis

Nitrogen adsorption–desorption surface area analysis was employed to determine the specific surface area, pore diameter, pore volume, pore size distribution, and adsorption–desorption isotherms of the synthesized samples. The analysis focused on Cu-TiO_2@TUD-C composites with copper dopant loadings of 0.1, 0.5, 0.7, and 1.0 mol%. Table 3 presents the measured surface area, pore diameter, and pore volume of each sample. An overall increase in surface area was observed with the rise in Cu dopant concentration, except for the 0.7 mol% Cu-TiO_2@TUD-C sample, which showed a slight deviation from this trend. According to the literature, pure TiO_2 possessed a surface area of approximately 21 m^2/g [4]. In contrast, the incorporation of TUD-C as a support matrix significantly enhanced the surface area of TiO_2, by more than 10-fold, as reflected in Table 3. This demonstrated the advantageous role of TUD-C. Furthermore, all analyzed samples exhibited pore diameters greater than 2 nm, confirming their mesoporous nature and successful integration of Cu-TiO_2 within the TUD-C framework, irrespective of the Cu dopant concentration on TiO_2 [4]. The observed increase in pore diameter can be attributed to the expansion of pore volume, which likely results from the accumulation of Cu-TiO_2 nanoparticles along the internal pore channels. This accumulation effect subsequently leads to a broadening of the pore structure [11].

Table 3 Surface area, pore volume, and pore diameter of TUD-C supported Cu-TiO_2 materials

Samples	Surface area (m^2/g)	Pore volume (cm^3/g)	Pore diameter (nm)
0.1 Cu-TiO_2@TUD-C	291	0.45	6.19
0.5 Cu-TiO_2@TUD-C	298	0.56	7.51
0.7 Cu-TiO_2@TUD-C	270	0.37	5.53
1.0 Cu-TiO_2@TUD-C	321	0.64	8.02

Figure 5 illustrates the nitrogen adsorption–desorption isotherms of Cu-doped TiO_2 supported on TUD-C with varying copper loadings (0.1, 0.5, 0.7, and 1.0 mol%). All Cu-TiO_2@TUD-C samples exhibited type IV isotherms accompanied by H4-type hysteresis loops [4], characteristic of mesoporous materials with narrow slit-like pores. Within the relative pressure range of $P/P_0 \approx 0.1$ to 0.5, the desorption branches of all samples closely followed their respective adsorption curves. This behaviour is attributed to mass transfer limitations arising from the irregular pore architecture, where structural constrictions hinder the uniform filling and emptying of adsorbate molecules [4,11]. Additionally, the presence of ultra-small mesopores adjacent to micropores contributed to the convergence of adsorption and desorption curves within this pressure interval. This dual-pore character is linked to the use of TEAOH as a structure-directing agent during hydrothermal synthesis, facilitating the formation of microporous features within the MFI zeolitic framework. Concurrently, the employment of TEA, a known silicon chelating agent, promoted the generation of mesopores through the formation of silicon atrane complexes, particularly during the ambient aging stage of the synthesis process [4,11]. A distinct hysteresis loop became evident for all the samples at P/P_0 Mean values exceeding 0.5. Furthermore, a stepwise shift in the isotherms within the range of P/P_0 = 0.55–1.0 was observed, providing compelling evidence for the negligible presence of macropores in the material structure [4].

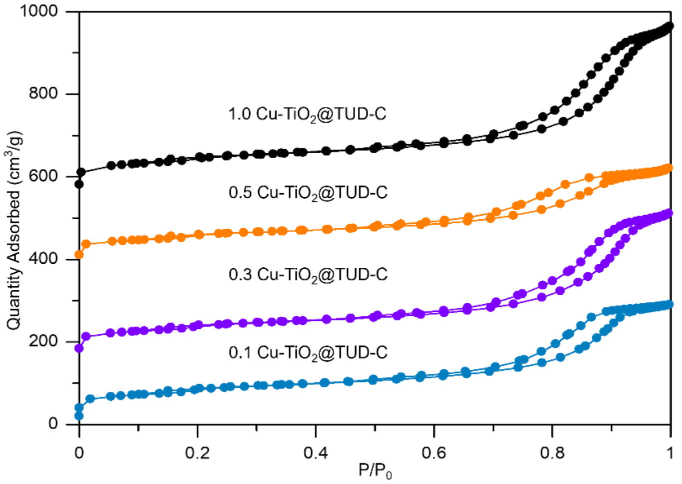

Figure 5 N_2 adsorption-desorption isotherms of *x*Cu-TiO_2@TUD-C (*x* = 0.1, 0.5, 0.7 and 1.0 mol%)

3.2.5 Field Emission Scanning Electron Microscopy (FESEM) and Energy Dispersive X-Ray (EDX) Analysis

FESEM was used to observe the synthesized samples' surface shape and structure. Figure 6 shows the FESEM images of 1.0Cu-TiO_2@TUD-C. From the images, the sample showed rough, uneven, and ball-like particles, which indicate that Cu-TiO_2 had clumped together. In addition, sponge-like structures that were not uniform or symmetrical could be seen in the image taken at 100x magnification [4]. The weight and atomic percentages of all elements are listed in Table 4. Both Ti and Cu elements in the 1.0Cu-TiO_2@TUD-C sample confirm that Cu-TiO_2 was successfully added to the TUD-C support. According to the EDX analysis, the empirical formula of the material was determined to be $CuTi_2AlSi_{250}C_{751}O_{1769}$. It should be noted that EDX is a qualitative analysis, and the high content of O could be due to environmental contamination.

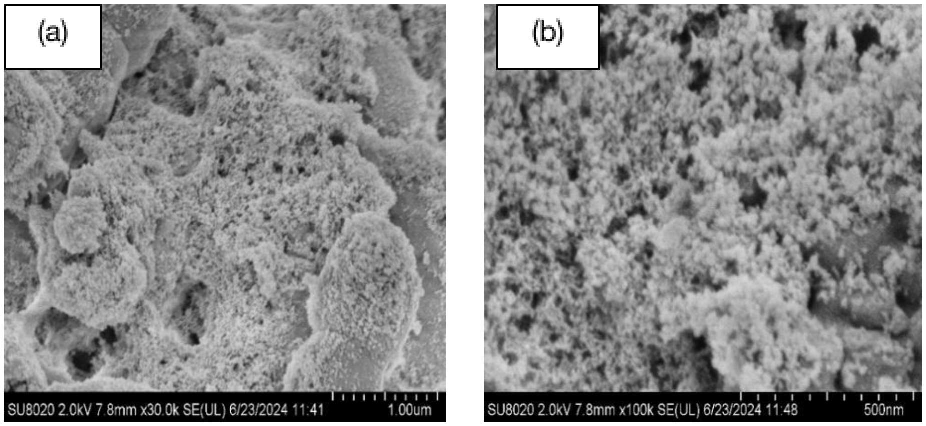

Figure 6 FESEM micrographs of 1.0 Cu-TiO_2@TUD-C with the magnification of (a) 30 x and (b) 100 x

Table 4 EDX elemental analysis of 1.0 Cu-TiO_2@TUD-C sample

Chemical composition	Weight percentage / %	Calculated atomic percentage / %
O	58.6	63.33
Si	26.1	16.07
C	14.0	20.16
Ti	0.6	0.22
Cu	0.6	0.16
Al	0.1	0.06

4.0 CONCLUSION

A series of Cu-TiO_2@TUD-C photocatalysts with varying copper dopant molar ratios was successfully synthesized through a multi-step approach, combining sol-gel, wet impregnation, hydrothermal treatment, and calcination processes. For comparative purposes, pristine TiO_2 and TUD-C were also prepared. The structural and physicochemical characteristics of the synthesized materials were thoroughly examined. Powder XRD and FTIR spectroscopy confirmed the formation of the MFI-type zeolitic framework across all TUD-C-supported samples. XRD patterns further revealed the co-existence of anatase-phase TiO_2 and monoclinic CuO in the Cu-TiO_2@TUD-C composites. Besides, DR Uv-Vis spectroscopy revealed that the Cu-TiO_2@TUD-C samples with 0.1, 0.5, and 0.7 mol% copper doping exhibited a notable reduction in band gap energies, with 2.93 eV, 3.06 eV, and 2.77 eV, respectively, lower than that of pristine TiO_2, which was recorded at 3.29 eV. On the other hand, nitrogen adsorption-desorption analysis verified that the TUD-C-based materials exhibited a high specific surface area. Additionally, energy-dispersive X-ray (EDX) spectroscopy affirmed the successful incorporation of Cu-TiO_2 onto the TUD-C support. The findings suggested that the prepared Cu-TiO_2@TUD-C materials are potential visible-light driven photocatalysts for degradation of various organic pollutants such as dyes, phenol, pharmaceuticals, etc.

Acknowledgment

The financial support obtained from the Ministry of Higher Education Malaysia (MOHE) and Universiti Teknologi Malaysia (UTM) through the Potential Academic Staff grant (Cost centre: QJ130000.2754.03K86) is acknowledged. The authors are grateful to the University Industry Research Laboratory, UTM, for the research facilities, including the XRD.

References

1. Eddy, D. R., Sheha, G. A. N., Permana, M. D., Saito, N., Takei, T., Kumada, N., Irkham, Rahayu, I., Abe, I., Sekine, Y., Oyumi, T., & Izumi, Y. (2024). Study on triphase of polymorphs TiO_2 (anatase/rutile/brookite) for boosting photocatalytic activity of metformin degradation. *Chemosphere, 351*, 141206. https://doi.org/10.1016/j.chemosphere.2024.141206
2. Wang, Y. Y., Chen, Y. X., Barakat, T., Zeng, Y. J., Liu, J., Siffert, S., & Su, B. L. (2022). Recent advances in non-metal doped titania for solar-driven photocatalytic/photoelectrochemical water-splitting. *Journal of Energy Chemistry, 66*, 529–559. https://doi.org/10.1016/j.jechem.2021.08.038
3. Wong, W. D., Majnis, M. F., Lai, C. W., Sagadevan, S., & Julkapli, N. M. (2024). Enhancement of mixing and reaction efficiency of various fluids applications at different microfluidic configuration and design. *Chemical Engineering and Processing - Process Intensification, 198*, 109729. https://doi.org/10.1016/j.cep.2024.109729
4. Ling, C. M., Teng, C. C., Hatta, M. H. M., & Lee, S. L. (2021). Tungsten oxide doped titania supported on TUD-C for photocatalytic removal of methylene blue. *Platform: A Journal of Science and Technology, 4*(2), 42–52. https://doi.org/10.61762/pjstvol4iss2art13217
5. Ling, C. M., Yuliati, L., Lintang, H. O., & Lee, S. L. (2020). TUD-C-supported tungsten oxide-doped titania catalysts for cyclohexane oxidation. *Malaysian Journal of Chemistry, 22*(2), 29–36.
6. Molahalli, V., Sharma, A., Bijapur, K., Soman, G., Shetty, A., Sirichandana, B., Patel, B. M., Chattham, N., & Hegde, G. (2024). *Copper-based nanomaterials in organic transformations*. Washington, DC: American Chemical Society.
7. He, L., Yang, Z., Xu, Y., Lu, X., Kaba, S., Li, C., Yao, X., Xu, D., & Yao, Z. (2024). Copper doped UiO-66@TiO_2 heterojunction for highly efficient photodegradation of odors in broiler houses. *Journal of Cleaner Production, 451*, 142103. https://doi.org/10.1016/j.jclepro.2024.142103
8. Albaidani, K., Timoumi, A., Belhadj, W., Alamri, S. N., & Ahmed, S. A. (2023). Structural, electronic and optical characteristics of TiO_2 and Cu-TiO_2 thin films produced by sol-gel spin coating. *Ceramics International, 49*(22), 36265–36275. https://doi.org/10.1016/j.ceramint.2023.08.309
9. Yang, Y., Shen, H., Ma, C., Li, D., Ma, B., Lu, Y., & Wang, Y. (2024). Preparation of C@CuNi/TiO_2 with a local surface plasmon resonance for photocatalytic degradation of organic dyes and antibiotics under visible light irradiation. *Colloids and Surfaces A: Physicochemical and Engineering Aspects, 703*, 135406. https://doi.org/10.1016/j.colsurfa.2024.135406
10. Duan, L., Lin, Q., Peng, H., Lu, C., Shao, C., Wang, D., Rao, S., Cao, H., & Lv, W. (2023). The catalytic reduction mechanisms of metal-doped TiO_2 for nitrate produced from non-thermal discharge plasma: The interfacial photogenerated electron transfer and reduction process. *Applied Catalysis A: General, 650*, 118995. https://doi.org/10.1016/j.apcata.2022.118995
11. Ooi, Y. K., Hussin, F., Yuliati, L., & Lee, S. L. (2019). Comparison study on molybdena-titania supported on TUD-1 and TUD-C synthesized via sol-gel templating method: Properties and catalytic performance in olefins epoxidation. *Materials Research Express, 6*(7), 074001. https://doi.org/10.1088/2053-1591/ab12be
12. Ooi, Y. K., Yuliati, L., Hartanto, D., Nur, H., & Lee, S. L. (2016). Mesostructured TUD-C supported molybdena doped titania as high selective oxidative catalyst for olefins epoxidation at ambient condition. *Microporous and Mesoporous Materials, 225*, 411–420. https://doi.org/10.1016/j.micromeso.2016.01.016

13. Nikitha, N., Raguram, T., Rajni, K. S., & Kuppusamy, M. (2025). Impact of Sn-Sr co-doping on structural, morphological and optical properties of TiO_2 for solar energy conversion applications. *Optik, 328*, 172332. https://doi.org/10.1016/j.ijleo.2025.172332
14. Nagarani, S., Sasikala, G., Yuvaraj, M., Kumar, R. D., Balachandran, S., & Kumar, M. (2022). ZnO-CuO nanoparticles enameled on reduced graphene nanosheets as electrode materials for supercapacitors applications. *Journal of Energy Storage, 52*, 104969. https://doi.org/10.1016/j.est.2022.104969
15. Saffari, M., Kavousi, Z. H., Ghorbanloo, M., Nada, A. A., Bekheet, M. F., Bezzerga, D., Hong, J., Morsali, A., Holade, Y., Viter, R., & El-Maghrabi, H. H. (2024). Copper benzene-1,3,5-tricarboxylate based metal organic framework (MOF) derived CuO/TiO_2 nanofibers and their use as visible light active photocatalyst for the hydrogen production. *Applied Surface Science, 678*, 161061. https://doi.org/10.1016/j.apsusc.2024.161061
16. Raguram, T., & Rajni, K. S. (2022). Synthesis and characterisation of Cu-doped TiO_2 nanoparticles for DSSC and photocatalytic applications. *International Journal of Hydrogen Energy, 47*(7), 4674–4689. https://doi.org/10.1016/j.ijhydene.2021.11.113
17. Huang, Q., Lou, X., Nie, D., Zhao, Z., Fan, K., Guo, W., Meng, J., Liu, Z., & Han, Z. (2024). Accelerated photodegradation of T-2 toxin over magnetic recyclable $ZnO/CaFe_2O_4$ nanocomposite with a pn based Z-scheme heterojunction architecture. *Separation and Purification Technology, 347*, 127518. https://doi.org/10.1016/j.seppur.2024.127518
18. Cheng, Z., Zheng, Q., Duan, Y., Cai, M., & Zhang, H. (2024). Effect of subcritical water temperature on the structure, antioxidant activity and immune activity of polysaccharides from *Glycyrrhiza inflata* Batalin. *International Journal of Biological Macromolecules, 261*, 129591. https://doi.org/10.1016/j.ijbiomac.2024.129591
19. Aslam, S., Subhan, F., Waqas, M., Zifeng, Y., Yaseen, M., & Naeem, M. (2023). Cu nanoparticles confined within ZSM-5 derived mesoporous silica (MZ) with enhanced stability for catalytic hydrogenation of 4-nitrophenol and degradation of azo dye. *Microporous and Mesoporous Materials, 354*, 112547. https://doi.org/10.1016/j.micromeso.2023.112547